Mon. Not. R. Astron. Soc. **337,** 981–992 (2002)

A Parkes half-Jansky sample of GHz peaked spectrum galaxies

I. A. G. Snellen,[1⋆] M. D. Lehnert,[2] M. N. Bremer[3] and R. T. Schilizzi[4,5]

[1]*Institute for Astronomy, Blackford Hill, Edinburgh EH9 3HJ*
[1]*Max-Planck-Institut für extraterrestrische Physik (MPE), Postfach 1312, 85741 Garching, Germany*
[3]*Department of Physics, Bristol University, H H Wills Physics Laboratory, Tyndall Avenue, Bristol BS8 1TL*
[4]*Joint Institute for VLBI in Europe, Postbus 2, 7990 AA, Dwingeloo, The Netherlands*
[5]*Leiden Observatory, PO Box 9513, 2300 RA, Leiden, The Netherlands*

Accepted 2002 August 13. Received 2002 August 12; in original form 2002 June 13

ABSTRACT

This paper describes the selection of a new southern/equatorial sample of gigahertz peaked spectrum (GPS) radio galaxies, and subsequent optical charge-coupled device imaging and spectroscopic observations using the ESO 3.6-m telescope. The sample consists of 49 sources with $-40^\circ < \delta < +15^\circ$, $|b| > 20^\circ$ and $S_{2.7\,\mathrm{GHz}} > 0.5$ Jy, selected from the Parkes PKSCAT90 survey. Approximately 80 per cent of the sources are optically identified, and approximately half of the identifications have available redshifts. The *R*-band Hubble diagram and evolution of the host galaxies of GPS sources are reviewed.

Key words: galaxies: active – radio continuum: galaxies.

1 INTRODUCTION

Gigahertz peaked spectrum (GPS) radio sources are a class of powerful compact extra-galactic radio source characterized by an overall turnover in their radio spectra at ∼1 GHz in frequency (for a review on GPS sources, see O'Dea 1998). They typically exhibit low flux density variability, implying that Doppler boosting is probably not important in these objects. This view is strengthened by the very long baseline interferometry (VLBI) morphologies – of at least those identified with galaxies (not GPS quasars) – which tend to show symmetric structures on both sides of a central core. These sources are therefore also called compact symmetric objects (CSO). The overlap between the two classes is large, but may not be complete (see Snellen, Schilizzi & van Langevelde 2000a for a discussion).

The characteristics of GPS sources are quite different from that of other classes of compact radio source, which can be highly variable, and are almost always dominated by Doppler-boosted, one-sided core-jet emission. This may also be the case for GPS sources optically identified with quasars that also show core-jet VLBI morphologies. It has been argued that the GPS galaxies and quasars may not be related at all, but just happen to have similar radio spectra (Snellen et al. 1999). In contrast to GPS galaxies, the GPS quasars are almost exclusively found at very high redshifts (O'Dea, Baum & Stanghellini 1991; Stanghellini et al. 1998; de Vries, Barthel & O'Dea 1997).

CSO and GPS galaxies have received considerable attention, because they are generally thought to be the young progenitors of large-size radio sources. Measurements of hotspot advance speeds (Owsianik & Conway 1998; Owsianik, Conway & Polatidis 1998; Taylor et al. 2000; Tschager et al. 2000) by multi-epoch VLBI observations have proven for a handful of archetype GPS sources that these objects are indeed young, typically 10^{2-3} yr. In addition, measurements of the high-frequency breaks in the slightly larger compact steep spectrum (CSS) radio sources, indicate that they have radiative ages in the range of 10^{3-5} yr (Murgia et al. 1999). It is therefore generally believed that GPS galaxies evolve into CSS and then FR I and/or FR II radio sources, assuming that they are fuelled for long enough. This makes CSO/GPS galaxies the key objects for studying the early evolution of powerful radio-loud active galactic nuclei (AGN) (Fanti et al. 1995; Readhead et al. 1996; O'Dea & Baum 1997; Snellen et al. 2000b).

Complete samples of GPS sources are vital to perform statistical studies. The complete sample of Stanghellini et al. (1998), containing sources with $S_{5\,\mathrm{GHz}} > 1$ Jy, is the most extensively studied. Other samples include the faint GPS sources of Snellen et al. (1998), and that with GPS sources from the JVAS survey (Marecki et al. 1999). Since radio telescopes are mostly situated in the northern hemisphere, radio surveys are also strongly biased towards the north. This hampers complete statistical studies of southern GPS sources, even at the highest flux density levels. Since the space density of GPS sources is so low, full sky coverage is important to firmly determine the behaviour of the high end of the luminosity function of GPS sources, which is vital for constraining radio source evolution models (Snellen et al. 2000b). In contrast, the most powerful optical telescopes are found in the south (at least those available to European scientists), and therefore it is of great value to have a significant and well-defined sample of GPS sources in the southern hemisphere. Pioneering work on southern GPS sources has been done by de Vries, Barthel & Hes (1995) and de Vries et al. (2000), especially on obtaining optical identifications and redshifts, and by

⋆E-mail: ignas@roe.ac.uk

King et al. (1996) involving VLBI observations, but their samples are not clearly defined. This paper describes the selection of a complete southern/equatorial sample of GPS galaxies from the Parkes PKSCAT90 data base (Otrupcek & Wright 1991), and presents the radio spectra and the optical identification status in a homogeneous way. Note that the GPS sources identified as quasars are not included in the sample. Section 2 describes the selection of the sample and its radio properties. Section 3 describes optical charge-coupled device (CCD) imaging and spectroscopy performed with the ESO 3.6-m telescope. In Section 4, the results are presented and discussed, including an update on the *R*-band Hubble diagram for GPS galaxies.

2 A SOUTHERN/EQUATORIAL SAMPLE OF GPS GALAXIES

2.1 Selection of the sample

The basis for the selection of sources in the sample is the Parkes multifrequency survey (PKSCAT90, Wright & Otrupcek 1990), which is a compilation of flux density measurements at frequencies of 178 MHz (4C), 408 MHz (Molonglo catalogue) and at 625, 1410, 2700, 5000 and 8400 MHz taken from the Parkes surveys. First, all sources with $S_{2700\,\mathrm{MHz}} > 0.5$ Jy were selected in the regions with $-40^\circ <$ Dec. $< +15^\circ$ and galactic latitude, $|b| > 20^\circ$ (1129 sources). This flux density limit and galactic latitude cut-off were chosen to be the same as those of the Parkes half-Jansky sample of flat spectrum radio sources (Drinkwater et al. 1997), allowing comparison of source statistics between the two samples. Note that most GPS galaxies are not found in the flat spectrum sample, since their high-frequency spectrum is too steep. Since 1410-MHz Parkes data are only sparsely available, the positions of these sources were cross-correlated with the NVSS survey (Condon et al. 1998), of which all flux density was included within a radius of 6 arcmin from the Parkes position. In addition, the sources were cross-correlated with the Texas 365-MHz survey (Douglas et al. 1996), which covers most of the sky area of the sample. Each spectrum was then fitted in an automated way with a second-order polynomial function to find objects with a possible turnover. A total of 323 objects were pre-selected all of which showed a maximum above 100 MHz in the resulting fit. The spectra of these objects were then inspected visually to judge the validity of the fit. The resulting 193 objects were cross-correlated with all Parkes radio sources in the NASA/IPAC Extra-galactic Data base (NED) with available redshifts (to filter out any quasars). The NED data base and the CATS data base of radio sources (Verkhodanov, Chernenkov & Trushkin 1997) were then searched extensively for additional flux density points and other information on the remaining 125 objects. In addition, the NVSS maps of each of the candidates were checked to see whether or not any extended emission was present. The low-frequency survey measurements were taken with interferometers, and therefore possible extended emission may have been missed. This indeed turned out to be a major source of contamination for many (47) mostly nearby radio galaxies. In other cases, the extra data points found in the NED and CATS data bases showed that the spectra did not turn over at frequencies below 300–400 MHz, or were subject to strong variability (19). A few candidates turned out to be planetary nebulae (three), and some were BL Lacs or quasars without a measured redshift (seven). The spectra of all sources that were not pre-selected (806 objects) were also visually inspected to see whether any candidates had been missed. The remaining sample contains 49 radio sources with peaked spectra, which are optically identified with a galaxy or still without an optical identification.

2.2 The radio properties of the sample

From the 49 sources in the resulting sample, 12 are also present in the brighter samples of GPS sources from Stanghellini et al. (1998) and de Vries et al. (2000). The properties of the objects are given in Table 1, with in column 1, the J2000 IAU name, in column 2 an alternative name, in column 3 the most accurate radio position found in the NED data base or that from the NVSS survey (on which the optical identification process is based), in column 4 the *R*-band magnitude (corrected to Cousins *R* and galactic extinction taken into account), in column 5 the redshift, in column 6 the flux density at 2700 MHz, in column 7 the turnover frequency, in column 8 the flux density at the turnover, in column 9 the reference for the magnitude, in column 10 the reference for the redshift and in column 11 a possible comment. The radio spectra are shown in Fig. 1. The solid lines indicate a second-order polynomial fit to the data points to guide the eye, and do not represent physically meaningful model fits. The turnover frequencies given in column 6 of Table 1 are often just estimates, since it was not possible to determine them accurately owing to the sparse sampling near their spectral peak.

3 OPTICAL ESO 3.6-m OBSERVATIONS

Optical CCD imaging and spectroscopy were performed on objects in the sample using the ESO 3.6-m telescope at La Silla, in Chile, on 2000 July 27–28, using the ESO Faint Object Spectrograph and Camera (EFOSC2). The weather was photometric throughout both nights. EFOSC2 uses a 2048 × 2048 thinned Loral CCD chip with a 0.157 pixel size, which was binned by 2 × 2 for both the imaging and spectroscopy.

3.1 CCD imaging

14 objects in the sample were observed in the *g*, *r* and/or *i* filters, which have effective wavelengths of 5169, 6814 and 7931 Å, respectively. For the flux density calibration standard star fields from Landolt (1992) were observed throughout the nights, and fluctuations in the magnitude scale zero-points were found to be smaller than 0.03 mag. The images were reduced in a standard way in the software package IRAF from the NOAO, but were positionally calibrated within the AIPS software package (from the NRAO) using the task XTRAN. Positions of bright stars in the CCD fields were taken from the APM catalogue (Irwin, Maddox & McMahon 1994) or the COSMOS UKST catalogue (Hambly et al. 2001), and in some cases directly measured on the second Digitized Sky Survey. The flux calibrator measurements in Landolt (1992) were performed in the Johnson–Kron–Cousins *UBVRI* photometric system, which is a somewhat different filter system from that used in this paper. The differences for the *R*- and *I*-band observations were found to be within the observational uncertainties, however, for the *g*-band observations, a colour correction to the *V*-band had to be applied. From the observations of the standard star fields, this colour correction was found to be $V = g - 0.44(V - R)$. The magnitudes of the optical identifications were determined by adding the flux within a box including all the emission from the object nearest the radio position. In the case of multiple objects near the radio positions (possible merging or interacting galaxy systems), the magnitudes were calculated for the total system and each component individually.

3.2 CCD spectroscopy

We used the EFOSC2 grism no 06, which has 600 gratings mm^{-1}, resulting in a dispersion of 2.06 Å pixel^{-1} and a wavelengths

Table 1. The radio and optical properties of objects in the southern/equatorial sample of GPS galaxies.

IAU name	Other name	Radio position (J2000)	m_R (mag)	z	$S_{2.7\mathrm{GHz}}$ (Jy)	ν_{peak} (GHz)	S_{peak} (Jy)	Ref. m_R	Ref. z	Comm.
J0022+0014	4C+00.02	00 22 25.48 + 00 14 56.0	18.10 ± 0.20	0.305	1.94	0.6	3.1	2	2	A
J0108–1201	B0105–122	01 08 13.20 − 12 00 50.3	22.39 ± 0.06		0.52	1.0	0.9	1		
J0206–3024	B0204–306	02 06 43.26 − 30 24 58.2	21.00 ± 0.50		0.58	0.5	0.9	13		
J0210+0419	B0208+040	02 10 44.52 +04 19 35.4	> 24.1		0.56	0.4	1.3	1		
J0210–2213	B0207–224	02 10 10.05 − 22 13 36.6	23.52 ± 0.13		0.86	1.5	1.1	1		
J0242–2132	B0240–217	02 42 35.87 − 21 32 26.2	17.10 ± 0.50	0.314	0.97	1.0	1.3	13	11	
J0323+0534	4C+05.14	03 23 20.27 +05 34 11.9	19.20 ± 0.50		1.60	0.4	7.1	13		
J0401–2921	B0359–294	04 01 21.50 − 29 21 26.1	> 21.0		0.58	0.4	1.0	13		
J0407–3924	B0405–395	04 07 34.43 − 39 24 47.2	20.40 ± 0.50		0.52	0.4	1.4	13		
J0407–2757	B0405–280	04 07 57.94 − 27 57 05.1	21.14 ± 0.04		0.93	1.5	1.4	1		
J0433–0229	4C–02.17	04 33 54.90 − 02 29 56.0	19.10 ± 0.50		1.04	0.4	3.0	13		
J0441–3340	B0439–337	04 41 33.80 − 33 40 03.6	> 21.0		0.88	1.5	1.2	13		
J0457–0848	B0454–088	04 57 20.24 − 08 49 05.2	20.30 ± 0.50		0.58	0.4	1.0	13		
J0503+0203	B0500+019	05 03 21.20 +02 03 04.6	$i21.0 \pm 0.20$	0.583	2.46	2.5	2.5	4	4	A
J0943–0819	B0941–080	09 43 36.86 − 08 19 32.0	17.50 ± 0.20	0.228	1.73	0.4	4.2	9	10	A
J0913+1454	B0910+151	09 13 35.00 +14 54 20.1	> 20.0		0.54	0.6	1.1	13		
J1044–2712	B1042–269	10 44 37.63 − 27 12 18.6	> 21.0		0.55	1.5	0.8	13		
J1057+0012	B1054+004	10 57 15.78 +00 12 03.7	> 21.0		0.58	0.4	1.6	13		
J1109+1043	B1107+109	11 09 46.04 +10 43 43.4	20.50 ± 0.50		0.80	0.5	2.4	13		E
J1110–1858	B1107–187	11 10 00.45 − 18 58 49.2	19.60 ± 0.20	0.497	0.65	1.0	0.9	8	12	
J1120+1420	4C+14.41	11 20 27.81 +14 20 55.0	20.10 ± 0.10	0.362	1.50	0.4	3.7	4	4	A
J1122–2742	B1120–274	11 22 56.41 − 27 42 48.2	> 21.0		0.74	1.4	0.8	13		
J1135–0021	4C–00.45	11 35 12.96 − 00 21 19.5	16.50 ± 0.50		0.76	0.4	2.9	13		D
J1203+0414	B1200+045	12 03 21.95 +04 14 17.7	18.80 ± 0.50		0.52	0.4	1.4	13		
J1345–3015	B1343–300	13 45 51.52 − 30 15 04.1	> 21.0		0.56	0.4	2.5	13		
J1347+1217	4C+12.50	13 47 33.36 +12 17 24.2	15.20 ± 0.20	0.122	3.88	0.4	8.8	2	2	A
J1350–2204	B1347–218	13 50 14.33 − 22 04 43.7	20.93 ± 0.05		0.72	0.4	1.4	1		
J1352+0232	B1349+027	13 52 30.68 +02 32 47.7	20.00 ± 0.50		0.78	0.4	2.0	13		
J1352+1107	4C+11.46	13 52 56.37 +11 07 07.7	> 21.0		0.78	0.4	3.6	13		
J1447–3409	B1444–339	14 47 19.69 − 34 09 16.2	21.00 ± 0.10		0.50	0.5	1.0	13		
J1506–0919	B1503–091	15 06 03.05 − 09 19 12.5	19.70 ± 0.50		0.87	0.6	1.6	13		
J1521+0430	4C+04.51	15 21 14.51 +04 30 20.0	22.10 ± 0.11	1.296	2.30	1.0	5.4	6	10	A
J1543–0757	B1540–077	15 43 01.69 − 07 57 03.6	17.40 ± 0.10	0.172	1.21	0.4	1.7	5	5	C
J1546+0026	B1543+005	15 46 09.50 +00 26 24.6	20.10 ± 0.20	0.556	1.24	0.6	2.2	2	5	C
J1548–1213	B1545–120	15 48 12.97 − 12 13 31.8	21.88 ± 0.13	0.883	1.45	0.4	3.7	1	1	
J1556–0622	4C–06.43	15 56 13.99 − 06 22 37.8	22.20 ± 0.13		0.77	0.4	2.4	1		
J1600–0037	B1557–004	16 00 00.91 − 00 37 23.3	–		0.54	1.0	1.2	1		F
J1604–2223	B1601–222	16 04 01.45 − 22 23 41.3	18.75 ± 0.10	0.141	0.57	0.6	1.0	5	1	
J1640+1220	4C+12.60	16 40 47.96 +12 20 02.1	21.36 ± 0.20	1.150	1.48	0.4	3.7	1	1	
J1648+0242	4C+02.43	16 48 31.79 +02 42 46.0	> 21.0		0.61	0.4	3.4	13		
J1734+0926	B1732+094	17 34 58.38 +09 26 57.8	20.80 ± 0.10		1.08	1.0	1.1	5		B
J2011–0644	B2008–068	20 11 14.22 − 06 44 03.6	21.18 ± 0.04	0.547	2.09	1.4	2.6	1	1	A
J2058+0540	4C+05.78	20 58 28.84 +05 42 50.7	23.40 ± 0.30	1.381	0.65	0.4	3.1	7	7	
J2123–0112	B2121–014	21 23 39.12 − 01 12 34.3	23.30 ± 0.10	1.158	0.64	0.4	2.0	3	2	
J2130+0502	B2128+048	21 30 32.88 +05 02 17.5	22.21 ± 0.07	0.990	3.12	1.0	4.8	1	10	A
J2151+0552	B2149+056	21 51 37.88 +05 52 13.0	20.20 ± 0.20	0.740	1.01	5.0	1.2	3	10	A
J2212+0152	4C+01.69	22 12 37.97 +01 52 51.7	$i22.0 \pm 0.20$		1.80	0.4	4.6	4		A
J2325–0344	B2322–040	23 25 10.23 − 03 44 46.7	23.50 ± 0.20		0.91	1.4	1.2	9		B
J2339–0604	4C–06.76	23 37 11.95 − 06 04 12.4	22.91 ± 0.20		0.80	0.4	3.8	1		

Comments:
(A) also in the sample of > 1 Jy GPS sources from Stanghellini et al. (1998); (B) also in the sample of de Vries e al. (1997) (C) Also in the sample of de Vries et al. (2000); (D) possibly a quasar; (E) large offset between the radio and optical position (F) near a bright star, no magnitude.
References:
(1) this paper; (2) Snellen et al. (1996); (3) O'Dea, Baum & Morris (1990); (4) de Vries et al. (1995); (5) de Vries et al. (2000).
(6) Biretta, Schneider & Gunn (1985); (7) Stern et al. (1999); (8) Fugmann, Meisenheimer & Roeser (1988); (9) Stanghellini et al. (1993); (10) Stanghellini et al. (1998); (11) Otrupcek & Wright (1991); (12) Drinkwater et al. (1997); (13) Digitized Sky Survey II; APM catalogue (Irwin et al. 1994); SuperCosmos Sky Surveys (Hambly et al. 2001).

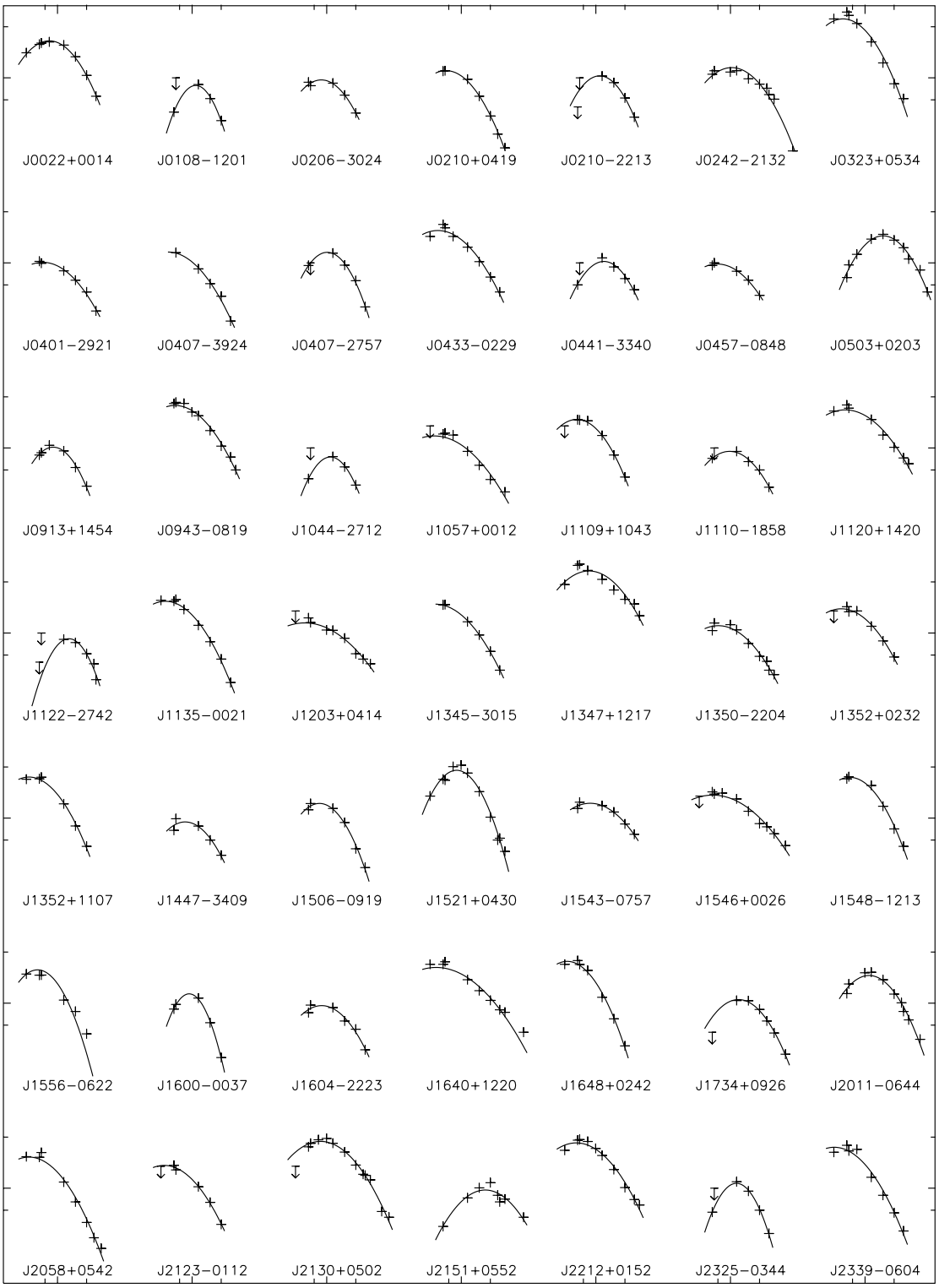

Figure 1. The radio spectra of the GPS galaxies in our sample. The tick-marks indicate 0.5, 1.0 and 5.0 GHz in frequency, and 0.5, 1.0 and 5.0 Jy in flux density.

coverage of 3860–8070 Å. A slit-width of 1 arcsec was used, resulting in a resolution of 13 Å. Usually the slit was oriented near the paralactic angle. The reduction of the spectra was carried out in a standard way using the IRAF NOAO reduction software. Wavelength calibration was carried out using a helium–argon lamp. One-dimensional spectra were extracted by summing in the spatial direction over an aperture as large as the spatial extent of the continuum or the brightest emission line.

3.3 Digitized sky surveys

If the object was not observed by us, and no optical observation was found in the literature, an image was extracted from the red second

Digitized Sky Survey. In addition, the APM catalogue (Irwin et al. 1994) and the SuperCosmos Sky Survey catalogues (Hambly et al. 2001) were searched for a possible identification and subsequently magnitude estimate. Unfortunately, the galaxy magnitudes in these catalogues are only accurate to ∼0.5 mag DSS2 data were retrieved for 22 sources (see Fig. A2 in the Appendix), with nine objects remaining unidentified.

4 RESULTS AND DISCUSSION

The photometric results of the imaging part of the EFOSC2 observations are given in Table 2, with in column 1 the source name, in columns 2 and 3 the exposure time and magnitude of the *V*-band observations, in columns 4 and 5 those of the observations in hte *R* band, and in columns 6 and 7 those of the *I*-band observations. The *R*-band images are shown in Fig. A1, except for J1604–2223, for which the *I*-band image is shown. Four objects (J0407–2757, J1350–2204, J1556–0622, J2011–0644) seem to have a close companion object. For these objects, the total magnitude of the system is given, and those of the individual components, with that closest to the radio position indicated with 'GPS' in column 1 of Table 2. Note that the magnitudes in Table 2 have not yet been corrected for galactic extinction.

The results of the spectroscopic part of the EFOSC2 observations are given in Table 3, with in column 1 the source name, in column 2 the exposure time and in columns 3–5 the name, observed wavelength and derived redshift of the identified spectral features, respectively. Only the galaxies for which spectral features could be identified and subsequently their redshift determined, are listed. Their spectra are shown in Fig. 2. Spectra of several other galaxies were taken, but did not show any identifiable features, and therefore no redshift could be determined. Clearly, these objects do not have emission lines of high equivalent width.

The ESO results and those of the DSS2 are incorporated in Table 1, with in column 4 the *R*-band magnitude, corrected for galactic extinction using the values of Schlegel, Finkbeiner & Davis (1998). The references to the optical magnitude and the redshift are given in columns 9 and 10. The final column of Table 1 gives possible comments. One source, J1109+1043, has a large offset between the radio and optical position, casting doubt on its possible optical identification. The radio source J1600–0037 is located too close (17 arcsec) to a 12th magnitude star to allow an identification. This object is therefore excluded from statistical analysis. The optical identification of J1135–0021 could be point-like and therefore may be a quasar. Strictly speaking it is not clear whether the empty fields are actually galaxies and not quasars. However, from the magnitude distribution of other samples of GPS sources, it is rather unlikely that they are quasars (most of the GPS quasars have $m_R < 21$). In general, only when all the sources are identified and spectra taken, can we be confident that all the objects are galaxies. The total identification fraction of the sample is ∼80 per cent. Approximately half of the identified objects have their redshifts determined.

Table 3. Details of the spectroscopic observations.

Name	t (s)	Spectral feature name	λ_{obs}	z
J1548–1213	1800			0.883 ± 0.001
		[O II] 3727 Å	7019	0.8833
		[Ne III] 3869 Å	7285	0.8829
J1604–2223	2700			0.141 ± 0.001
		G 4300 Å	4909	0.1416
		mgb 5169 Å	5898	0.1410
		Na 5899 Å	6727	0.1404
		Hβ 4861 Å	5549	0.1415
J1640+1220	4800			1.150 ± 0.003
		Mg II 2798 Å	6015	1.1497
		[C II] 2326 Å	5010	1.1539
		[C III] 4101 Å	1909	1.1482
J2011–0644	4200			0.547 ± 0.001
		[O II] 3727 Å	5766	0.5471
		break 4000 Å	6150	0.54

Table 2. Details of the CCD imaging observations.

Name	*V* band		*R* band		*I* band	
	t (s)	m_V (mag)	t (s)	m_R (mag)	t (s)	m_I (mag)
J0108–1201	60	23.50 ± 0.23	120	22.45 ± 0.06	300	22.15 ± 0.15
J0210–2213	60	> 24.40	1500	23.55 ± 0.13	300	23.68 ± 0.32
J0210+0419			1500	> 24.20		
J0407–2757	60	21.94 ± 0.19	60	21.24 ± 0.04		
GPS-west		22.61 ± 0.16		21.71 ± 0.11		
East		22.87 ± 0.20		22.12 ± 0.13		
J1350–2204	60	21.99 ± 0.07	300	21.13 ± 0.05	300	20.30 ± 0.12
GPS-north		23.33 ± 0.29		22.04 ± 0.08		20.89 ± 0.08
South		22.59 ± 0.12		21.93 ± 0.10		21.50 ± 0.13
J1548–1213	60	22.93 ± 0.17	300	22.52 ± 0.13	300	21.55 ± 0.11
J1556–0622	60	> 23.40	1500	22.82 ± 0.13	1500	22.33 ± 0.06
East				23.40 ± 0.15		22.93 ± 0.13
GPS-west				23.80 ± 0.17		23.26 ± 0.17
J1604–2223	60	21.24 ± 0.05			300	18.53 ± 0.03
J1640+1220			60	21.48 ± 0.20		
J2011–0644	60	22.81 ± 0.08	1500	21.52 ± 0.04	300	20.48 ± 0.06
North				22.06 ± 0.04		21.28 ± 0.08
GPS-south				22.48 ± 0.07		20.99 ± 0.07
J2130+0502			1500	22.38 ± 0.07	750	21.05 ± 0.03
J2339–0604			210	23.00 ± 0.20	600	22.12 ± 0.09

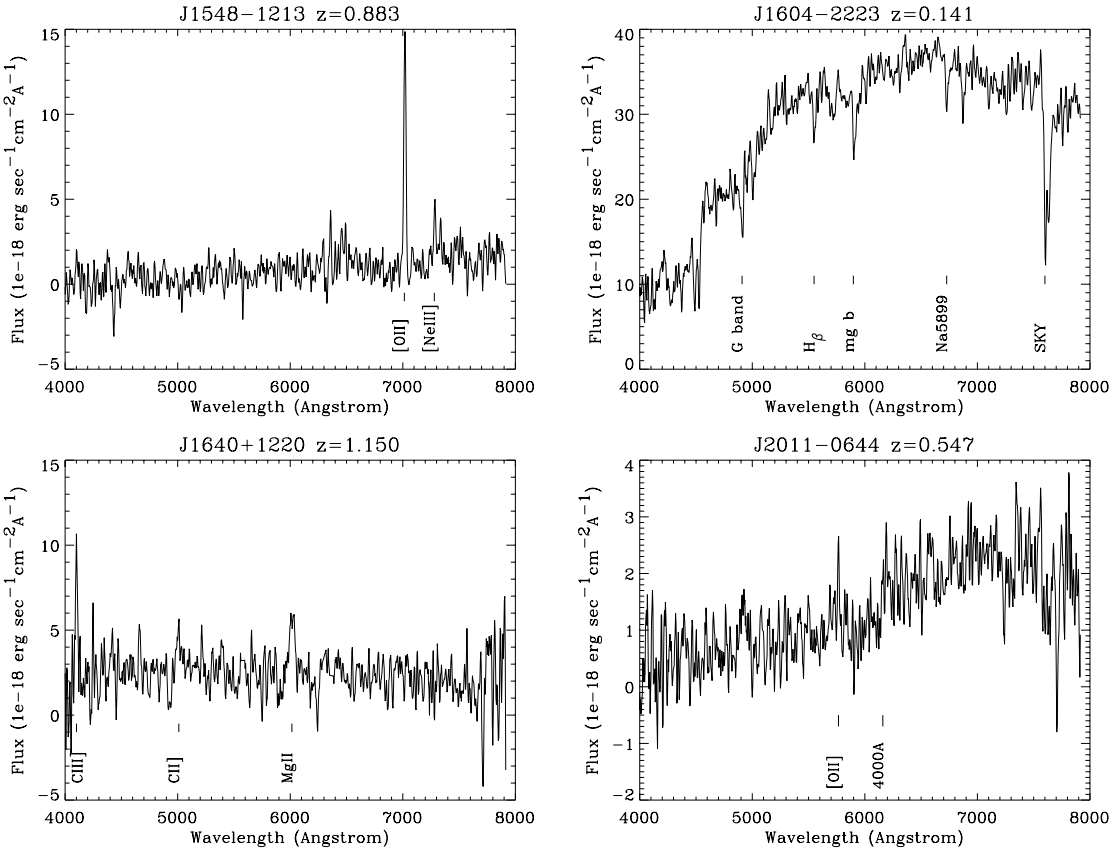

Figure 2. Optical spectra taken with EFOSC2 on the ESO 3.6-m telescope. Identified spectral features are indicated.

4.1 The magnitude distribution

The apparent magnitude of a (GPS) galaxy is closely related to its redshift, as will be discussed later. Therefore, the magnitude distribution of a GPS galaxy sample is a reflection of its redshift distribution. This distribution is very interesting, since it is closely related to the birth-function of radio galaxies and the cosmological evolution of the GPS luminosity function (Snellen et al. 2000b). The cumulative magnitude distribution is shown in Fig. 3, with the shaded area indicating the distribution of the half-Jansky sample (taking into account the uncertainty of the magnitudes of the objects without optical identification). GPS sources with $S_{2.7\mathrm{GHz}} > 1$ Jy were excluded to avoid overlap with the bright sample. The dashed line shows the magnitude distribution of the GPS galaxies of the >1 Jy (at 5 GHz) sample of Stanghellini et al. (1998), which is completely identified, and the dotted lines indicate the limits of the magnitude distribution of the galaxies in the faint GPS sample of Snellen et al. (1998). The mean flux density of the GPS sample of Stanghellini is approximately a factor of 4 brighter, and that of the faint GPS sample a factor of 6 fainter than the half-Jansky sample (with $S_{2.7\mathrm{GHz}} < 1$ Jy). Fig. 3 clearly shows that radio samples containing generally fainter radio sources are associated with galaxy samples with fainter magnitudes, with the median magnitudes of the bright, half-Jansky and faint samples being approximately 20, 21 and 22 in R, respectively. This seems to indicate that the radio-fainter GPS galaxies are primarily at higher redshift, and not simply with a lower radio luminosity.

4.2 The Hubble diagram, optical colours and absolute magnitudes

The Hubble diagram of GPS galaxies has been discussed previously by Snellen et al. (1996a,b) and O'Dea et al. (1996). Our group has claimed that the apparent magnitude–redshift relation of GPS galaxies shows a low dispersion, and that they are apparently fainter at high redshift than 3C objects. This has been interpreted in terms of the GPS galaxies being intrinsically redder than 3C galaxies, possibly because of the lack of the extra, blue light associated with the radio-optical alignment effect (Chambers, Miley & van Breugel 1987; McCarthy et al. 1987; Best, Longair & Röttgering 1997). This view is strengthened by observations that the optical to near-infrared colours of GPS galaxies are consistent with the light of these hosts being dominated by old stellar populations (O'Dea et al. 1996; Snellen et al. 1996b). In addition, Best, Longair & Röttgering (1998) show that 3C galaxies are typically up to a couple of magnitudes bluer in $R-K$ magnitudes than expected for passively evolving elliptical models. The lack of luminosity evolution found out to $z=1$, which would be expected for passively evolving ellipticals, was interpreted as a possible dynamical evolution of the systems through accretion, as found for brightest cluster galaxies (Aragon-Salamanca, Baugh & Kauffmann 1998). Note that most faint ($R \sim 24$) GPS galaxies are found to have $R-K \sim 5$–6 (Snellen et al. 1996b; 1998), and can therefore be classified as extremely red objects (ERO). Given their relative ease of selection, GPS galaxies promise to be excellent objects for studying the evolution of massive ellipticals out to $z > 1$.

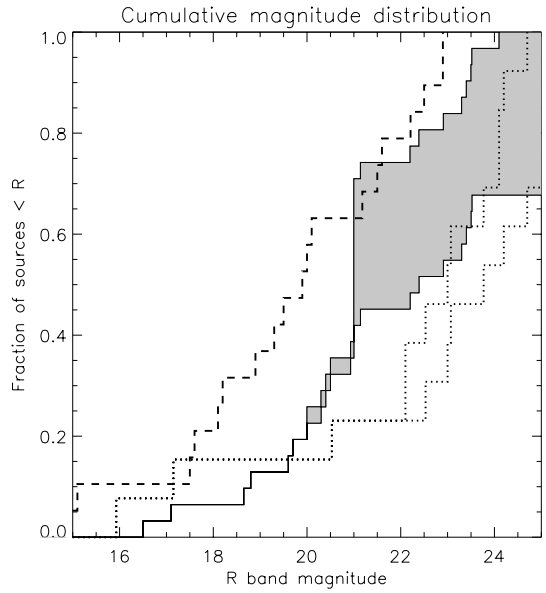

Figure 3. The cumulative *R*-band magnitude distribution of the half-Jansky sample of GPS galaxies, with the grey area indicating the uncertainty caused by the empty fields. The dashed line indicates the same distribution for the bright 1-Jy Stanghellini et al. (1998) sample, and the dotted lines the limits to that of the faint GPS sample of Snellen et al. (1998).

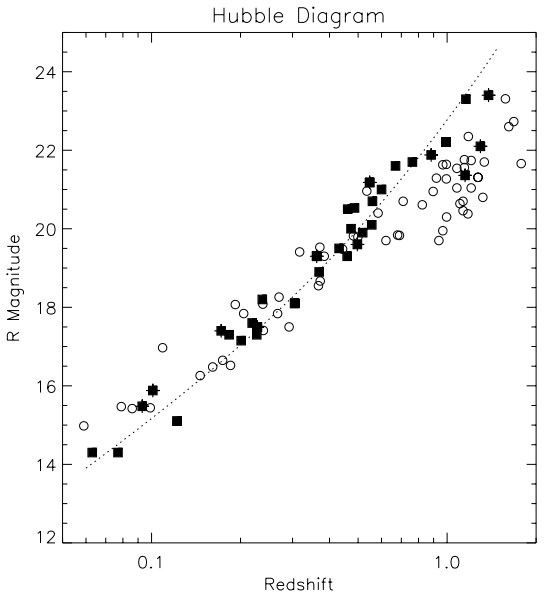

Figure 4. The Hubble diagram of GPS galaxies (solid squares) and 3C galaxies (open circles). The dotted line indicates the Hubble relation for GPS galaxies as found by Snellen et al. (1996). The crossed GPS galaxies are those new to the sample.

The combined samples of Stanghellini et al. (1998), Snellen et al. (1998) and that presented in this paper provide an additional 15 GPS galaxies with available redshifts, compared with the original analysis of the *R*-band Hubble diagram of Snellen et al. (1996a). A few galaxies have only rough estimates of their R magnitude from the DSS surveys and are excluded from the analysis below, leaving 34 galaxies in total (the galaxy J2151+0552 was excluded as well, since its optical light is strongly influenced by non-thermal emission). The updated Hubble diagram of GPS galaxies (solid squares) is shown in Fig. 4, in which all magnitudes are converted to Cousins *R*. The dotted line indicates the Hubble relation as fitted to the original data set in Snellen et al. (1996a). The open circles indicate 3C galaxies from a compilation of samples from Best et al. (1997), Eales (1985), and de Koff et al. (1996) with, if necessary, the magnitudes converted to 'total magnitudes' in *R* Cousins. As found before, the distant GPS galaxies are apparently fainter than 3C galaxies at similar redshift, which can be accounted for by the extra light of the alignment effect in 3C galaxies (e.g. Best et al. 1997). However, some differences from the original picture now emerge. On average, the nearby objects seem to be fainter than in the original sample, and the galaxies at $z > 1$ seem to be brighter than the original Hubble diagram indicates.

Fig. 5 shows the $R - I$ colours as a function of redshift, with sources taken from Stanghellini et al. (1993), Snellen et al. (1999) and this paper (all corrected to Cousins *R*). The shaded area indicates the expected $R - I$ colours for a passively evolving elliptical with a formation redshift of $z = 5$, and a range from one to two times the solar metallicity value (Worthey 1994). The $R - I$ colours are more or less as expected for passively evolving ellipticals, as shown previously by O'Dea et al. (1996).

Fig. 6 presents the absolute magnitudes for GPS galaxies (solid squares) and 3C galaxies (open circles). A cosmology with $H_0 = 70$ km s^{-1} Mpc^{-1}, $\Omega_\lambda = 0.3$ and $\Omega_m = 0.7$ is assumed, and the magnitudes are *K*-corrected using a synthetic galaxy spectrum by Worthey (1994) for a 12-Gyr old elliptical with solar metallicity. The

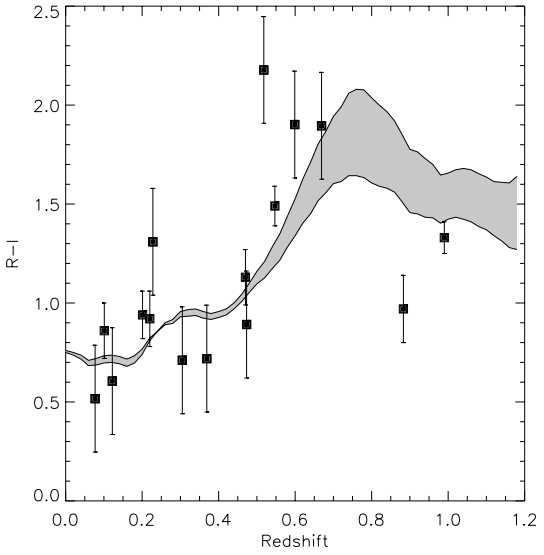

Figure 5. The $R - I$ colours as function of redshift for GPS galaxies taken from Stanghellini et al. (1993), Snellen et al. (1998) and this paper.

models of Worthey (1994) are also used to calculate the grey area, which represents the expected luminosity evolution as a function of redshift for a $2L_*$ elliptical with a formation redshift of $z = 5$, and a range of metallicities from one to two times the solar value.

As for the Hubble diagram, this picture seems to be different from that found earlier for the absolute *K*-band magnitudes of GPS galaxies as a function of redshift (Snellen et al. 1996b), which show a more or less constant absolute magnitude as a function of redshift. We believe this occurs for several reasons. First, the few low-redshift GPS galaxies available in 1996 seem to have been, on average, overluminous with respect to the general low-redshift population. This was already a concern at that time, since two of them have a Seyfert nucleus (4C+12.45 and B1404+286). This has moved the $z = 0$

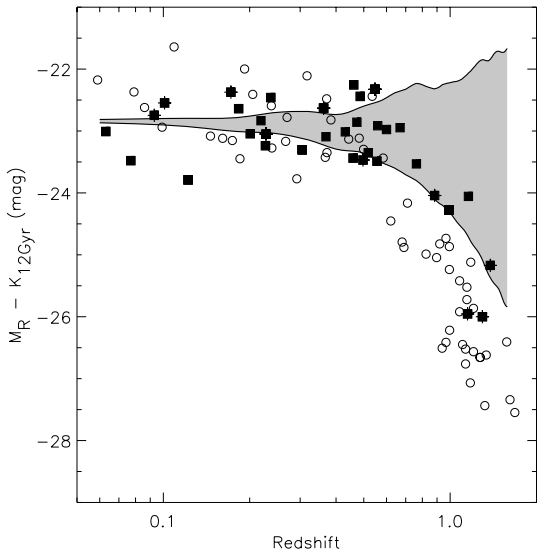

Figure 6. The absolute magnitudes of the host galaxies of GPS sources (solid squares) and 3C galaxies (open circles) as function of redshift. The magnitudes are *k*-corrected using a synthetic spectrum of a 12-Gyr old elliptical with solar metallicity from Worthey (1994). The crossed GPS galaxies are those new to the sample.

baseline to a lower luminosity, making the higher-redshift objects relatively brighter. Secondly, the now popular λ-cosmology makes the objects at a redshift of unity intrinsically approximately half a magnitude brighter as well. Thirdly, the newly measured redshifts at $z > 1$ are strongly biased towards the objects with the strongest emission lines, making contamination from an active nucleus more likely. It is therefore expected that the majority of the objects at $z > 1$, for which we were not able to determine a redshift, are intrinsically less luminous than the few objects shown in Figs 1 and 6. Indeed, from the four spectra shown in Fig. 2, the emission lines of the two galaxies at low redshift have very low equivalent widths, while those of the two at high redshift have a very high equivalent width. For that reason only the redshifts of the latter two could be determined. Several deep spectra of other faint galaxies were taken with no lines detected. 8-m class telescope time will be needed to resolve this issue.

4.3 Mergers and interactions

Previous work has indicated that disturbed optical morphologies and the presence of close companions are common characteristics of GPS galaxies (Stanghellini et al. 1993; O'Dea et al. 1996). Using a sample of radio-bright GPS galaxies, O'Dea et al. find that approximately half of the galaxies have disturbed morphologies and approximately one-fifth show a second component within a few arcsec. Very similar percentages have been found by Heckman et al. (1986) for a general sample of powerful radio-loud AGN. If GPS sources evolve into large-scale radio sources, then it their galactic environments would be expected to be similar, since the time-scales of interaction and/or mergers are larger than that of the lifetime of a radio source.

The statistics in the sample presented here are not yet good enough to perform a similar statistical analysis. However, it is interesting to note that of the 12 galaxies we imaged, four are clearly part of a multiple system (J0407–3924, J1350–2204, J1556+0622 and J2011–0644). In addition, J1548–1213 seems to have a second component, but the picture is less clear owing to two foreground stars nearby. At first glance, this gives a similar fraction of multiple systems to O'Dea et al. (1996) and Heckman et al. (1986). It is also interesting to note that in all four of the multiple systems, the GPS radio sources are identified with the redder component of the two. A more extensive observing programme for optical imaging and spectroscopy is planned.

5 SUMMARY AND CONCLUSIONS

In this paper we have described the selection of a new southern/equatorial sample of GPS radio galaxies, and presented subsequent optical CCD imaging and spectroscopic observations using the ESO 3.6-m telescope. The sample consists of 49 sources with $-40^\circ < \delta < +15^\circ$, $|b| > 20^\circ$ and $S_{2.7\mathrm{GHz}} > 0.5$ Jy, selected from the Parkes PKSCAT90 survey. Approximately 80 per cent of the sources are now optically identified, and approximately half of the identifications have their redshifts determined. The *R*-band Hubble diagram and evolution of the host galaxies of GPS sources are reviewed. The view on GPS galaxies seems to be slightly altered, with the host galaxies increasing in optical luminosity with redshift, as expected for passive evolution. This change appears to be caused by the low-z galaxies being less luminous than previously thought, the new λ-cosmology used and a strong observational bias towards high-redshift GPS galaxies being those with strong emission lines.

The sample presented in this paper has the potential to greatly improve the statistics on luminous young radio-loud AGN, and the use of hosts of GPS sources for galaxy evolution studies, especially with the VLT and Gemini-south telescopes.

ACKNOWLEDGMENTS

This research has made use of observations collected at the ESO/La Silla 3.6-m telescope, and of the NASA/IPAC Extragalactic Data Base (NED) which is operated by the Jet Propulsion Laboratory, California Institute of Technology, under contract with the National Aeronautics and Space Administration. We made use of the CATS data base (Verkhodanov et al. 1997) of the Special Astrophysical Observatory. The Second Palomar Observatory Sky Survey (POSS-II) was made by the California Institute of Technology with funds from the National Science Foundation, the National Aeronautics and Space Administration, the National Geographic Society, the Sloan Foundation, the Samuel Oschin Foundation, and the Eastman Kodak Corporation.

REFERENCES

Aragon-Salamanca A., Baugh C.M., Kauffmann G., 1998, MNRAS, 297, 427
Best P.N., Longair M.S., Röttgering H.J.A., 1997, MNRAS, 292, 758
Best P.N., Longair M.S., Röttgering H.J.A., 1998, MNRAS, 295, 549
Biretta J.A., Schneider D.P., Gunn J.E., 1985, AJ, 90, 250
Chambers K.C., Miley G.K., van Breugel W., 1987, Nat, 329, 604
Condon J.J., Cotton W.D., Greisen E.W., Yin Q.F., Perley R.A., Taylor G.B., Broderick J.J., 1998, AJ, 115, 1693
Douglas J.N., Bash F.N., Bozyan F.A., Torrence G.W., Wolfe C., 1996, AJ, 111, 1945
Drinkwater M.J. et al., 1997, MNRAS, 284, 85
de Koff S., Baum S.A., Sparks W.B., Biretta J., Golombek D., Macchetto F., McCarthy P., Miley G.K., 1996, ApJS, 107, 621
de Vries W.H., Barthel P.D., Hes R., 1995, A&AS, 114, 259
de Vries W.H., Barthel P.D., O'Dea C.P., 1997, A&A, 321, 105

de Vries W.H., O'Dea C.P., Barthel P.D., Thompson D.J., 2000, A&AS, 143, 18
Eales S.A., 1985, MNRAS, 213, 899
Fanti C., Fanti R., Dallacasa D., Schilizzi R.T., Spencer R.E., Stanghellini C., 1995, A&A, 302, 317
Fugmann W., Meisenheimer K., Roeser H.-J., 1988, A&AS, 75, 173
Hambly N.C. et al., 2001, MNRAS, 326, 1279
Heckman T.M., Smith E.P., Baum S.A., van Breugel W.J.M., Miley G.K., Illingworth G.D., Bothun G.D., Balick B., 1986, ApJ, 311, 526
Irwin M., Maddox S., McMahon R., 1994, Spectrum, 2, 14
King A.E. et al., 1996, in Snellen I., Schilizzi R.T., Röttgering H.J.A., Bremer M.N., eds, Proc. 2nd Workshop on GPS and CSS Radio Sources, p. 17
Landolt A.U., 1992, AJ, 104, 340
Marecki A., Falcke H., Niezgoda J., Garrington S.T., Patnaik A.R., 1999, A&AS, 135, 273
McCarthy P.J., van Breugel W., Spinrad H., Djorgovski S., 1987, ApJ, 321, 29
Murgia M., Fanti C., Fanti R., Gregorini L., Klein U., Mack K-H., Vigotti M., 1999, A&A, 345, 769
O'Dea C.P., 1998, PASP, 110, 493
O'Dea C.P., Baum S.A., 1997, AJ, 113, 148
O'Dea C.P., Baum S.A., Morris G.B., 1990, A&A, 82, 261
O'Dea C.P., Baum S.A., Stanghellini C., 1991, ApJ, 380, 66
O'Dea C.P., Stanghellini C., Baum S.A., Charlot S., 1996, ApJ, 470, 806
Otrupcek R., Wright A., 1991, PASA, 9, 170
Owsianik I., Conway J.E., 1998, A&A, 337, 69
Owsianik I., Conway J.E., Polatidis A.G., 1998, A&A, 336, L37
Readhead A.C.S., Taylor G.B., Xu W., Pearson T.J., Wilkinson P.N., 1996, ApJ, 460, 634
Schlegel D.J., Finkbeiner D.P., Davis M., 1998, ApJ, 500, 525
Snellen I.A.G., Bremer M.N., Schilizzi R.T., Miley G.K., van Ojik R., 1996a, MNRAS, 279, 1294
Snellen I.A.G., Bremer M.N., Schilizzi R.T., Miley G.K., 1996b, MNRAS, 283, 123
Snellen I.A.G., Schilizzi R.T., de Bruyn A.G., Miley G.K., Rengelink R.B., Röttgering H.J.A., Bremer M.N., 1998, A&AS, 131, 435
Snellen I.A.G., Schilizzi R.T., Bremer M.N., Miley G.K., de Bruyn A.G., Röttgering H.J.A., 1999, MNRAS, 307, 149
Snellen I.A.G., Schilizzi R.T., van Langevelde H.J., 2000a, MNRAS, 319, 429
Snellen I.A.G., Schilizzi R.T., Miley G.K., de Bruyn A.G., Bremer M.N., Röttgering H.J.A., 2000b, MNRAS, 319, 445
Stanghellini C., O'Dea C.P., Baum S.A., Laurikanen E., 1993, ApJS, 88, 1
Stanghellini C., O'Dea C.P., Dallacasa D., Baum S.A., Fanti R., Fanti C., 1998, A&AS, 131, 303
Stern D., Dey A., Spinrad H., Maxfield L., Dickinson M., Schlegel D., Gonzlez R.A., 1999, AJ, 117, 1122
Taylor G.B., Marr J.M., Pearson T.J., Readhead A.C.S., 2000, ApJ, 541, 112
Tschager W., Schilizzi R.T., Röttgering H.J.A., Snellen I.A.G., Miley G.K., 2000, A&A, 360, 887
Verkhodanov O.V., Trushkin S.A., Andernach H., Chernenkov V.N., 1997, in Hunt G., Payne H.E., eds, ASP Conf. Ser. Vol. 125, Astronomical Data Analysis Software and Systems VI. Astron. Soc. Pac., San Francisco, p. 322
Worthey G., 1994, ApJS, 95, 107

APPENDIX: OPTICAL IMAGES

Images from the ESO 3.6-m observatories are shown in Fig A1 and from the red second Digitized Sky Survey in Fig A2.

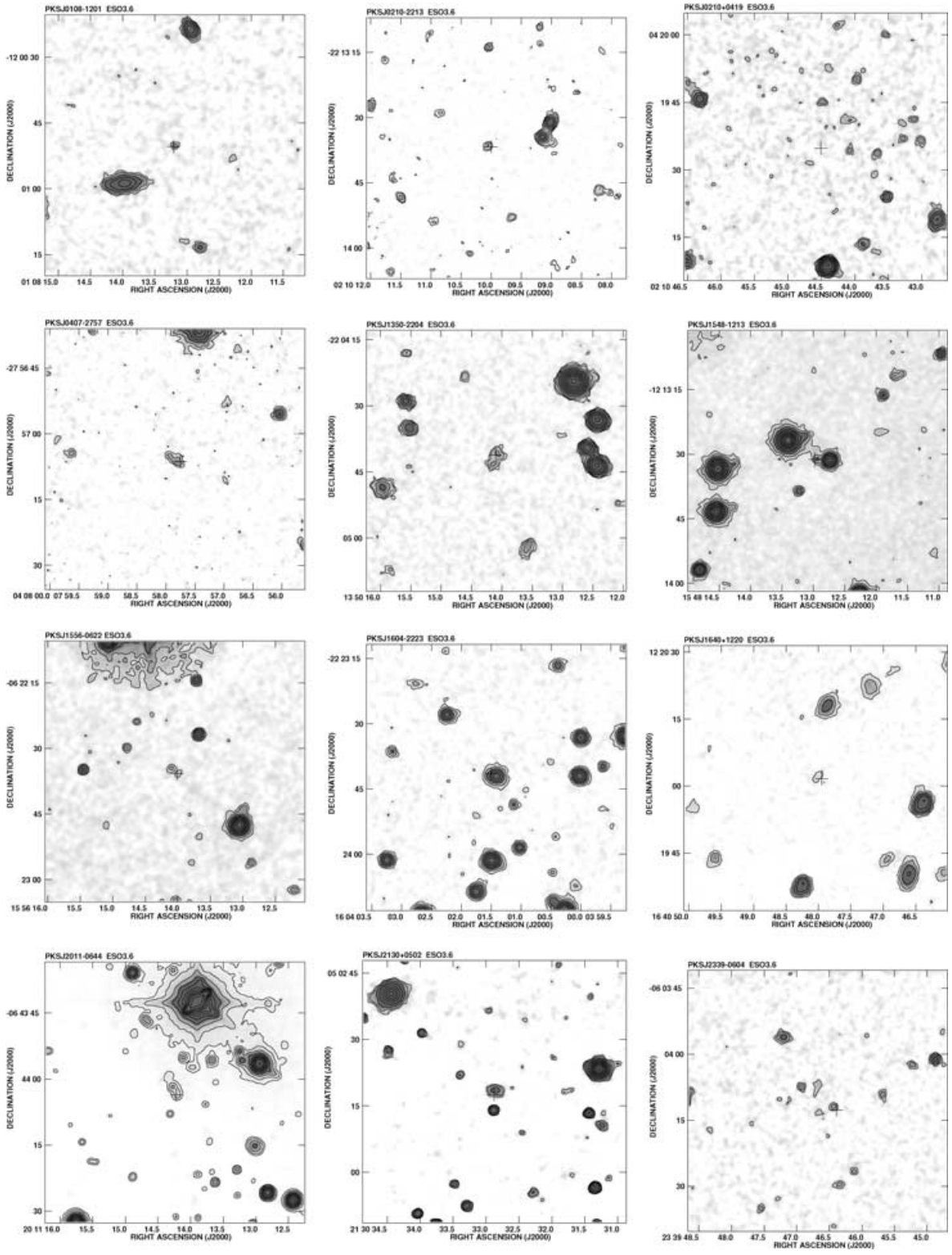

Figure A1. Images from the ESO 3.6-m observations.

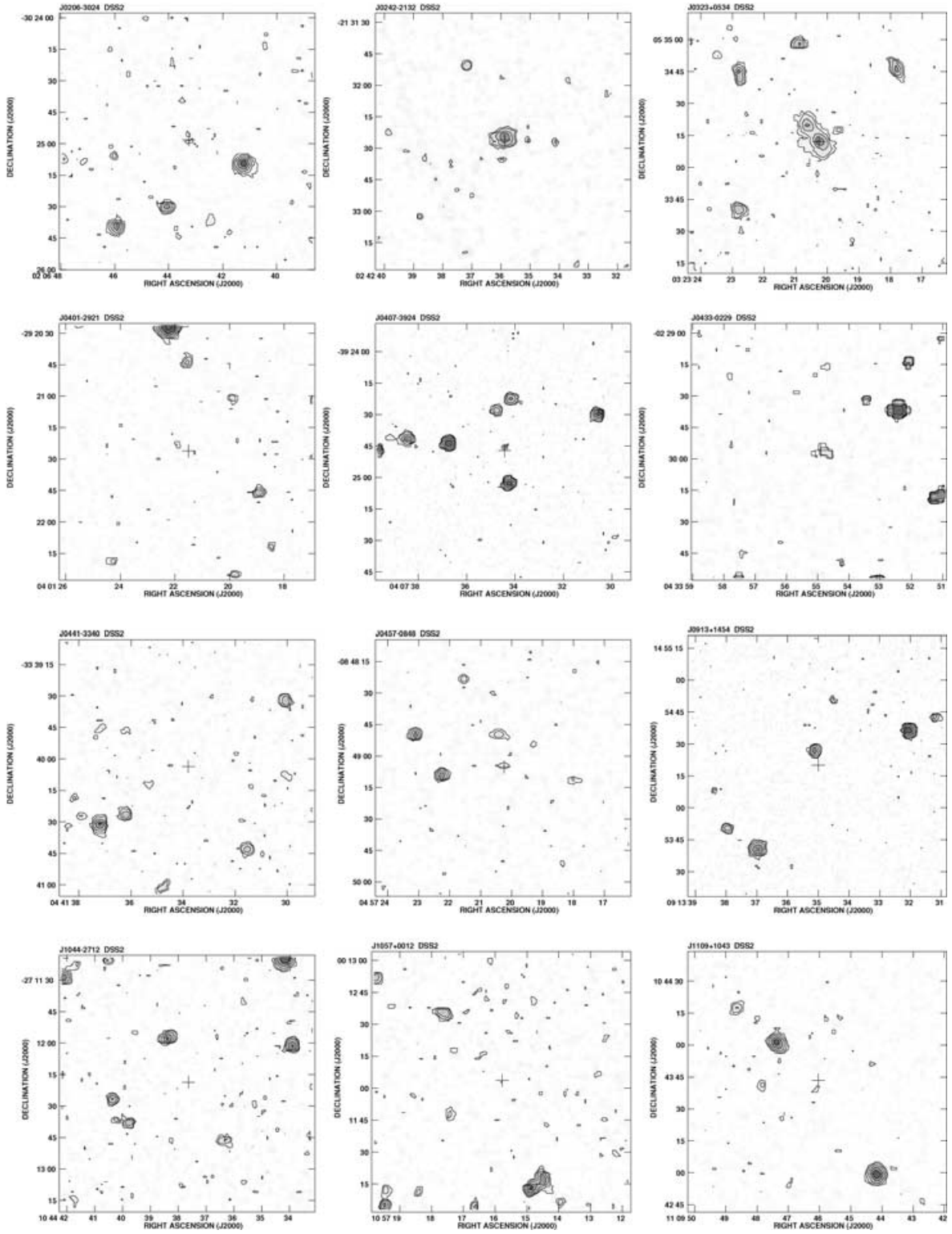

Figure A2. Images retrieved from the red second Digitized Sky Survey.

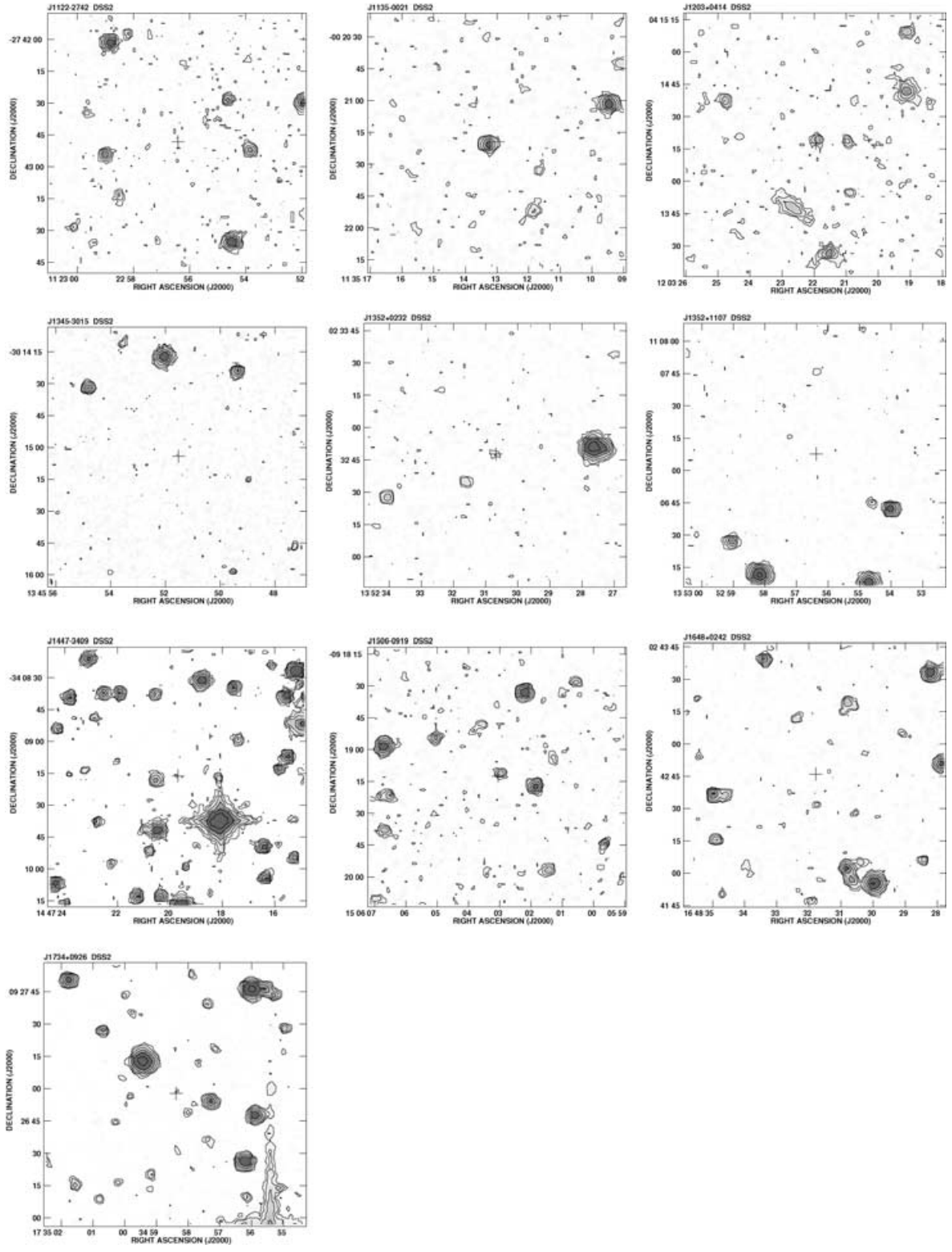

Figure A2 – *continued*

This paper has been typeset from a TEX/LATEX file prepared by the author.